Unimolecular Chemistry of Li^+- and Na^+-Coordinated Polyglycol Radicals, a New Class of Distonic Radical Cations

Jianglin Wu, Michael J. Polce, and Chrys Wesdemiotis*

Contribution from the Department of Chemistry, The University of Akron, Akron, Ohio 44325-3601

Received June 9, 2000

Abstract: The lithium and sodium ion complexes of the polyglycol-derived radicals ($R^•$) $HOCH_2CH_2O^•$ (**1**$^•$), $H(OCH_2CH_2)_2O^•$ (**2**$^•$), $HOCH_2CH_2OCH_2^•$ (**3**$^•$), $H(OCH_2CH_2)_2OCH_2^•$ (**4**$^•$), $HOCH_2CH_2OCH_2CH_2^•$ (**5**$^•$), and $H(OCH_2CH_2)_2OCH_2CH_2^•$ (**6**$^•$) are produced in the gas phase by fast atom bombardment ionization and their structures and unimolecular chemistry are investigated by tandem mass spectrometry. Parallel ab initio MO calculations show that the $[R^• + X]^+$ (X = Li, Na) complexes carry their positive charge and unpaired electron at distinct centers, thus representing a novel type of distonic radical cations. Radical reactions prevail for all $[R^• + X]^+$ species studied. The predominant dissociation of metalated **1**$^•$−**4**$^•$ (−O$^•$ or $-OCH_2^•$ terminus) involves cleavage of CH_2═O via ion−molecule complexes in which the newly detached formaldehyde molecule remains bound to the metal ion. With Li^+ cationization, H$^•$ transfer within these intermediate complexes also takes place, leading to the elimination of OCH$^•$; this reaction is particularly competitive at low internal energy. In sharp contrast to **1**$^•$−**4**$^•$, metalated **5**$^•$ and **6**$^•$ ($-OCH_2CH_2^•$ terminus) primarily decompose by 1,4- and 1,5-H$^•$ rearrangements, followed by cleavage of $^•CH_3$ and $^•C_2H_5$ radicals, and with **6**$^•$, also $HOCH_2^•$ and $HOCH_2CH_2^•$ radicals; at higher internal energies, the direct cleavage of CH_2═CH_2 becomes a further significant dissociation channel. Although the metal ion does not directly participate in the observed reactions, it plays an important role in either promoting or impeding specific radical-induced bond cleavages and H$^•$ rearrangements by (1) preventing bond rotations in R$^•$ (through coordination), (2) allowing for the formation of intermediary metal ion-bound heterodimer complexes, and (3) influencing the energetics of the radical site decompositions.

Introduction

Radical cations, in which the charge and radical sites reside at different locations, have been termed *distonic*;[1,2] they formally arise by electron removal from diradicals or zwitterions of the same connectivity.[1,2] Since theory predicted in the early eighties that distonic ions should exist as stable species in the gas phase,[3,4] the intrinsic chemistry of a large number of such ions has been studied extensively by both computations as well as mass spectrometry experiments.[4−21] The considerable interest devoted so far to distonic ions is due to several reasons, inter alia: (a) they are key intermediates in the fragmentation of the molecular ions of many organic molecules;[3−9,12−14,16−18] (b) they often are thermodynamically and kinetically more stable than isomeric conventional radical ions, thereby causing the latter to readily rearrange into distonic forms;[3,6,12,13,16−18] (c) the separate charge and radical sites make distonic ions ideally suitable reagents for tailored ion−molecule reactions that specifically probe the chemistry of either reactive center;[10,12,15] and (d) with well-stabilized charge centers, radical reactivity prevails.[7,11,15,19] In such systems, the charge provides a means to study the gas-phase chemistry of radical sites by mass spectrometry, an ideally suitable method for the separation and identification of the complex mixtures usually generated in radical reactions.[7,19]

The distonic radical cations characterized so far have mainly been organic ions or ions containing elements from groups 4A−5A.[1−19] The only metalated species known are the organometallic ions $^+FeC_6H_4^•$ (C_6H_4 = *o*-, *m*-, or *p*-benzyne).[20,21] This article presents the first comprehensive gas-phase study of distonic ions carrying main group metals, involving the com-

(1) Radom, L.; Bouma, W. J.; Nobes, R. H.; Yates, B. F. *Pure Appl. Chem.* **1984**, *12*, 1831−1842.
(2) Yates, B. F.; Bouma, W. J.; Radom, L. *Tetrahedron* **1986**, *42*, 6225−6234.
(3) Bouma, W. J.; MacLeod, J. K.; Radom, L. *J. Am. Chem. Soc.* **1980**, *102*, 2246−2252.
(4) Bouma, W. J.; Nobes, R. H.; Radom, L. *J. Am. Chem. Soc.* **1982**, *104*, 2929−2930.
(5) (a) Bouma, W. J.; MacLeod, J. K.; Radom, L. *J. Am. Chem. Soc.* **1982**, *104*, 2930−2931. (b) Holmes, J. L.; Lossing, F. P.; Terlouw, J. K.; Burgers, P. C. *J. Am. Chem. Soc.* **1982**, *104*, 2931−2932.
(6) Wesdemiotis, C.; Danis, P. O.; Feng, R.; Tso, J.; McLafferty, F. W. *J. Am. Chem. Soc.* **1985**, *107*, 8059−8066.
(7) Weiske, T.; Schwarz, H. *Tetrahedron* **1986**, *42*, 6245−6251.
(8) Bouchoux, G. *Mass Spectrom. Rev.* **1988**, *7*, 1−39 and 203−255.
(9) Hammerum, S. *Mass Spectrom. Rev.* **1988**, *7*, 123−202.
(10) Dass, C.; Gross, M. L. *Org. Mass Spectrom.* **1990**, *25*, 24−32.
(11) Stirk, K. M.; Kenttämaa, H. I. *J. Am. Chem. Soc.* **1991**, *113*, 5880−5881.
(12) Stirk, K. M.; Kiminkinen, L. K. M.; Kenttämaa, H. I. *Chem. Rev.* **1992**, *92*, 1649−1665.
(13) Polce, M. J.; Cordero, M. M.; Wesdemiotis, C.; Bott, P. A. *Int. J. Mass Spectrom. Ion Processes* **1992**, *113*, 35−58.
(14) Polce, M. J.; Wesdemiotis, C. *J. Am. Chem. Soc.* **1993**, *115*, 10849−10856.
(15) Van Amsterdam, M. W.; Zappey, H. W.; Ingemann, S.; Nibbering, N. M. M. *Org. Mass Spectrom.* **1993**, *28*, 30−36.
(16) Smith, R. L.; Chou, P. K.; Kenttämaa, H. I. In *The Structure, Energetics and Dynamics of Organic Ions*; Baer, T., Ng, C. Y., Powis, I., Eds.; John Wiley & Sons Ltd.: Chichester, 1996; pp. 197−280.
(17) Polce, M. J.; Wesdemiotis, C. *J. Am. Soc. Mass Spectrom.* **1996**, *7*, 573−589.
(18) Polce, M. J.; Wesdemiotis, C. *Rapid Commun. Mass Spectrom.* **1996**, *10*, 235−241.
(19) Thoen, K. K.; Smith, R. L.; Nousiainen, J. J.; Nelson, E. D.; Kenttämaa, H. I. *J. Am. Chem. Soc.* **1996**, *118*, 8669−8676.
(20) Xu, Y. C.; Freiser, B. S. *J. Am. Chem. Soc.* **1995**, *117*, 5413−5414.
(21) Xu, Y. C.; Chen, Q.; Poehlein, S. K.; Freiser, B. S. *Rapid Commun. Mass Spectrom.* **1999**, *13*, 645−649.

10.1021/ja0020660 CCC: $19.00
Published on Web 12/05/2000

Scheme 1

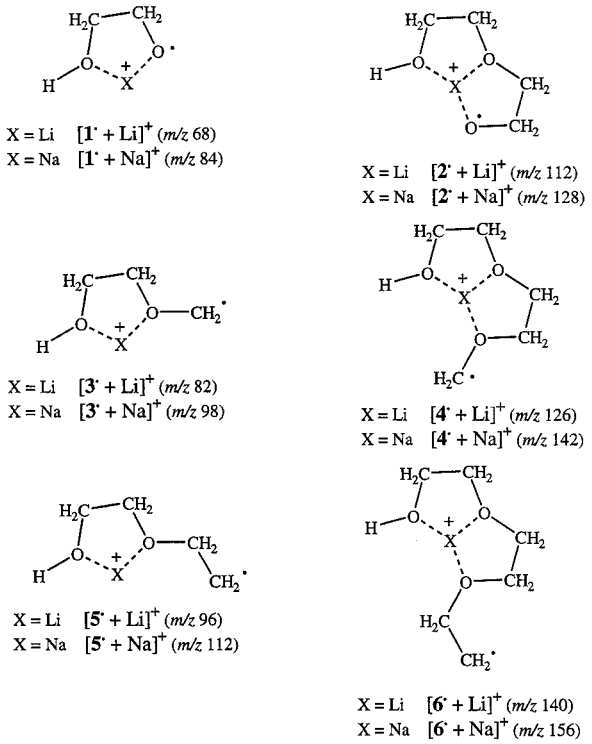

plexes between the alkali metal ions Li^+ and Na^+ and the poly(ethylene glycol)-derived methyl, ethyl, and ethoxy radicals ($R^•$) $HOCH_2CH_2O^•$ (2-hydroxyethoxy, **1**•), $H(OCH_2CH_2)_2O^•$ (2-(2′-hydroxyethoxy)ethoxy, **2**•), $HOCH_2CH_2OCH_2^•$ ((2-hydroxyethoxy)methyl, **3**•), $H(OCH_2CH_2)_2OCH_2^•$ (2-(2′-hydroxyethoxy)-ethoxymethyl, **4**•), $HOCH_2CH_2OCH_2CH_2^•$ (2-(2′-hydroxyethoxy)-ethyl, **5**•), and $H(OCH_2CH_2)_2OCH_2CH_2^•$ (2-[2′-(2′′-hydroxyethoxy)ethoxy]ethyl, **6**•). The unimolecular chemistry of these metal ion-coordinated radicals is explored by a palette of tandem mass spectrometry methods,[22,23] including metastable ion (MI) characteristics,[24] collisionally activated dissociation (CAD),[22,23] and three-stage mass spectrometry (MS^3).[23]

Previous studies in this[25] and other[26,27] laboratories have shown that CAD of the alkali metal ion adducts of polyglycols produces a series of fragments by elimination of radicals from one chain end. These decompositions proceed with maximum efficiency at high (keV) collision energy;[25] under such conditions, the most abundant products from the Li^+ and Na^+ adducts of poly(ethylene glycol) oligomers encompass the putative distonic radical ions depicted in Scheme 1, which are the subject of our investigation. Depending on the number of O atoms in these distonic ions, the metal ion can be ligated in a bi- or tridentate fashion.[28,29] Further, based on the polyglycol bond cleaved upon distonic ion formation, three different types of radical termini are possible, viz. $-O^•$ (oxy), $-OCH_2^•$ (methyl), and $-OCH_2CH_2^•$ (ethyl), cf. Scheme 1. Here, we examine in detail the effects of radical type and degree of metal ion ligation on the unimolecular reactions of the radical complexes $[R^• + Li]^+$ and $[R^• + Na]^+$. The experiments are complemented by ab initio molecular orbital theory to corroborate the viability of the $[R^• + X]^+$ (X = Li, Na) structures given in Scheme 1 and elucidate selected fragmentation pathways of such distonic ions.

Methods

Tandem Mass Spectrometry. All experiments were conducted with a modified Micromass AutoSpec mass spectrometer of E_1BE_2 geometry.[13] This instrument houses one collision cell (Cls-1) in the field-free region preceding E_1 (FFR-1) and two more (Cls-2 and Cls-3), with an intermediate ion deflector, in FFR-3. For metastable ion (MI) and collisionally activated dissociation (CAD) spectra of source-generated ions (MS^2), E_1B was used for precursor ion selection (MS-1) and E_2 for *m/z* analysis of the products formed in FFR-3 (MS-2). The precursor ions were accelerated to 8 keV (or as stated) before mass-selection by MS-1. Their CAD (MS^2) spectra were obtained by pressurizing Cls-3 with O_2. In MS^3 experiments, the precursor ion was generated in FFR-1 by CAD with He (Cls-1) and transmitted, by proper adjustment of E_1 and B, into FFR-3 where its CAD (MS^3) spectrum was acquired.

Kinetic energy releases of MI signals were calculated from peak widths at half-height ($T_{0.5}$) using established procedures.[24,30,31] In CAD (MS^2 and MS^3) experiments, the pressure of each collision gas was raised until the precursor ion intensity was reduced by ca. 20%. The spectra shown are multiscan summations and reproducible to within ±10%. The compounds introduced into the mass spectrometer were purchased from Aldrich and the collision gases from Linde (oxygen) and Liquid Carbonic (helium); all chemicals were used as received.

Molecular Orbital Calculations. The structures of the smaller $[R^• + Li]^+$ radical cations included in Scheme 1 as well as plausible isomeric structures were optimized by ab initio calculations at the HF/6-31G level; vibrational frequencies and zero-point vibrational energies were also obtained at this level. The energetics of selected dissociations of $[\mathbf{3}^• + X]^+$ were evaluated at the same level to substantiate proposed mechanisms. All calculations were performed on a pentium PC using Gaussian 94[32] for Windows interfaced with CHEM-3D.[33]

Results and Discussion

Synthesis of the Metalated Distonic Ions. The metal ion-coordinated radicals were formed via fast atom bombardment (FAB) ionization of poly(ethylene glycol) 200 (PEG 200) saturated with Li or Na salts. A few (1−2) microliters of the appropriate mixture were placed on the stainless steel probe tip, inserted into the mass spectrometer, and bombarded with 12 keV Cs^+ ions. The secondary ions ejected upon this process include $[M + X]^+$ (M = PEG oligomer; X = Li or Na) and their fragments, among them the nominal $[R^• + X]^+$ distonic radical ions depicted in Scheme 1. The most abundant $[M + X]^+$ contain the PEG tetramers, pentamers, and hexamers.

As mentioned in the Introduction, CAD of $[M + X]^+$ gives rise to abundant metalated radical ions via radical losses from one end of the polyglycol chain.[25] This is exemplified for

(22) McLafferty, F. W., Ed. *Tandem Mass Spectrometry*; Wiley: New York, 1983.
(23) Busch, K. L.; Glish, G. L.; McLuckey, S. A. *Mass Spectrometry/Mass Spectrometry*; VCH: New York, 1988.
(24) Cooks, R. G.; Beynon, J. H.; Caprioli, R. M.; Lester, G. R. *Metastable Ions*; Elsevier: Amsterdam, 1973.
(25) Selby, T. L.; Wesdemiotis, C.; Lattimer, R. P. *J. Am. Soc. Mass Spectrom.* **1994**, *5*, 1081−1092.
(26) Lattimer, R. P. *J. Am. Soc. Mass Spectrom.* **1992**, *3*, 225−234.
(27) Lattimer, R. P. *J. Am. Soc. Mass Spectrom.* **1994**, *5*, 1072−1080.
(28) (a) More, M. B.; Glendening, E. D.; Ray, D.; Feller, D.; Armentrout, P. B. *J. Phys. Chem.* **1996**, *100*, 1605−1614. (b) Ray, D.; Feller, D.; More, M. B.; Glendening, E. D.; Armentrout, P. B. *J. Phys. Chem.* **1996**, *100*, 16116−16125.
(29) More, M. B.; Ray, D.; Armentrout, P. B. *J. Phys. Chem. A* **1997**, *101*, 831−839. More, M. B.; Ray, D.; Armentrout, P. B. *J. Am. Chem. Soc.* **1999**, *121*, 417−423.
(30) Holmes, J. L.; Terlouw, J. K. *Org. Mass Spectrom.* **1980**, *15*, 383−396.
(31) Holmes, J. L. *Org. Mass Spectrom.* **1985**, *20*, 169−183.
(32) *Gaussian 94, Revision B. 1*; Frisch, M. J.; Trucks, G. W.; Schlegel, H. B.; Gill, P. M. W.; Johnson, B. G.; Robb, M. A.; Cheesemann, J. R.; Keith, T. A.; Peterson, G. A.; Montgomery, J. A.; Raghavachari, K.; Al-Laham, M. A.; Zakrewski, V. G.; Ortiz, J. V.; Foresman, J. B.; Cioslowski, J.; Stefanov, B. B.; Nanayakkara, A.; Challocombe, M.; Peng, C. Y.; Ayala, P. Y.; Chen, W.; Wong, M. W.; Andres, J. L.; Replogle, E. S.; Gomperts, R.; Martin, R. L.; Fox, D. J.; Binkley, J. S.; Defrees, D. J.; Baker, J.; Stewart, J. J. P.; Head-Gordon, M.; Gonzales, C.; Pople, J. A.; Gaussian, Inc.: Pittsburgh, PA, 1995.
(33) CambridgeSoft Corporation, Cambridge, MA.

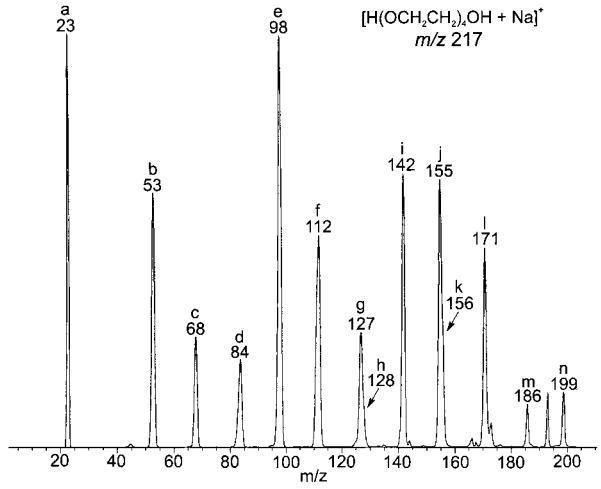

Figure 1. CAD spectrum of FAB-generated $[H(OCH_2CH_2)_4OH + Na]^+$. The fragments marked a−n correspond to the following: (a) Na^+; (b) $^+NaO{=}CH_2$; (c) loss of $^\bullet O(CH_2CH_2O)_3H$; (d) loss of $^\bullet CH_2$-$CH_2O(CH_2CH_2O)_2H$, $[\mathbf{1}^\bullet + Na]^+$; (e) loss of $^\bullet CH_2O(CH_2CH_2O)_2H$, $[\mathbf{3}^\bullet + Na]^+$; (f) loss of $^\bullet O(CH_2CH_2O)_2H$, $[\mathbf{5}^\bullet + Na]^+$; (g) loss of CH_3CH_2-OCH_2CH_2OH; (h) loss of $^\bullet CH_2CH_2OCH_2CH_2OH$, $[\mathbf{2}^\bullet + Na]^+$; (i) loss of $^\bullet CH_2OCH_2CH_2OH$, $[\mathbf{4}^\bullet + Na]^+$; (j) loss of $HOCH_2CH_2OH$; (k) loss of $^\bullet OCH_2CH_2OH$, $[\mathbf{6}^\bullet + Na]^+$; (l) loss of CH_3CH_2OH; (m) loss of $^\bullet CH_2OH$; and (n) loss of H_2O.

$[H(OCH_2CH_2)_4OH + Na]^+$ in Figure 1, where the radical losses and all other dominant fragment ions are annotated in the figure legend. The sodiated radicals investigated ($\mathbf{1}^\bullet$−$\mathbf{6}^\bullet$) are also identified in the figure legend. CAD (MS^3) on any of these $[R^\bullet + Na]^+$ ions leads to spectra that are indistinguishable from those obtained by CAD of source-generated ions of the same *m*/*z* and kinetic energy. This also applies to the $[R^\bullet + Li]^+$ ions studied. Hence, FAB ionization of PEG 200 generates the same metalated distonic ions as CAD of mass-selected $[M + X]^+$ oligomers. In the present study, the metalated radicals were formed by direct FAB ionization which produces $[R^\bullet + X]^+$ with higher yields and higher kinetic energies (higher transmission and collection efficiencies) than the alternative synthetic route via CAD.

Theoretical Assessment of the $[R^\bullet + X]^+$ Structures. To corroborate the postulated $[R^\bullet + X]^+$ structures, the geometries and electronic properties of the smaller lithiated complexes $[\mathbf{1}^\bullet + Li]^+$, $[\mathbf{3}^\bullet + Li]^+$, and $[\mathbf{5}^\bullet + Li]^+$ (left side of Scheme 1) as well as of selected isomers of these ions were investigated by ab initio theory. Radicals $\mathbf{1}^\bullet$, $\mathbf{3}^\bullet$, and $\mathbf{5}^\bullet$ contain two oxygen atoms, either of which is a potential binding site for the alkali metal cation. The optimized structures resulting after Li^+ attachment at just one or both of these basic centers are displayed in Figure 2. All isomers correspond to energy minima, but the relative energies of the bidentate species are substantially lower than those of their isomeric monodentate complexes. From the monodentate arrangements, the one resulting from Li^+ attachment to the hydroxyl group (center row) is more stable because it permits the formation of a hydrogen bond between the hydroxyl proton and the ether (or $O^\bullet$) oxygen. Such H bonding, which lowers the energy by ∼30 kJ mol^{-1}, cannot take place when Li^+ is bound to the ether (or $O^\bullet$) oxygen (top row) due to the decreased electron-donating capabilities of this O atom. Interconversion of the linear to the more stable cyclic isomers should be facile, as it only requires bond rotations and the disruption of weak hydrogen bonds. The much higher thermodynamic stability of the multidentate isomers supports our proposition that the $[R^\bullet + X]^+$ ions synthesized from PEG 200 have cyclic structures with the maximum possible number of ligands, as shown in Scheme 1.

Table 1. Charge and Electron Spin Distributions in $[R^\bullet + Li]^+$ [a]

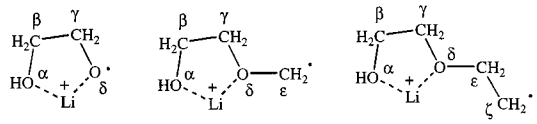

	$[\mathbf{1}^\bullet + Li]^+$		$[\mathbf{3}^\bullet + Li]^+$		$[\mathbf{5}^\bullet + Li]^+$	
	charge	spin	charge	spin	charge	spin
α-O	−0.877	0.000	−0.872	0.000	−0.868	0.000
α-H	+0.487	0.000	+0.484	0.000	+0.480	0.000
β-C	−0.021	+0.014	−0.010	0.000	−0.009	0.000
β_1-H	+0.240	0.000	+0.235	0.000	+0.225	+0.001
β_2-H	+0.239	−0.003	+0.231	0.000	+0.230	0.000
γ-C	−0.078	−0.133	+0.012	−0.007	+0.023	+0.009
γ_1-H	+0.270	+0.065	+0.232	+0.002	+0.214	−0.001
γ_2-H	+0.266	+0.025	+0.231	+0.005	+0.219	−0.001
δ-O	−0.387	**+1.044**	−0.846	−0.009	−0.855	+0.024
ε-C			+0.042	**+1.214**	−0.006	−0.159
ε_1-H			+0.200	−0.108	+0.213	+0.035
ε_2-H			+0.201	−0.098	+0.209	+0.007
ζ-C					−0.323	**+1.280**
ζ_1-H					+0.201	−0.107
ζ_2-H					+0.216	−0.108
Li	**+0.861**	−0.012	**+0.860**	+0.001	**+0.831**	+0.020

[a] Mulliken charge distributions and atomic spin densities based on ab initio MO calculations at the HF/6-31G level. Within each ion, the sum of Mulliken charges or spin densities is equal to 1. The bold numbers give the locations of highest charge and spin density within each ion.

Strong interactions between the metal ion and the O atoms of $R^\bullet$ are also predicted by the Mulliken charge distributions of the $[R^\bullet + Li]^+$ ions, which are given in Table 1. The largest positive charge is concentrated on Li, while the oxygens carry the largest negative charges, indicating favorable electrostatic bonding between these centers.

Based on the atomic spin densities of the $[R^\bullet + Li]^+$ radical cations (Table 1), the unpaired electron is essentially localized at the $O^\bullet$ atom in $[\mathbf{1}^\bullet + Li]^+$ and the C atom of the terminal $^\bullet CH_2$ group in $[\mathbf{3}^\bullet + Li]^+$ and $[\mathbf{5}^\bullet + Li]^+$. As mentioned above, the positive charge primarily resides on the metal atom and, hence, at a location distant from the radical site. As a result, $[R^\bullet + X]^+$ indeed represent distonic ions and $[\mathbf{1}^\bullet + X]^+$, where the charge and radical centers are adjacent, also qualifies as an ylide ion.[1]

Metal Ion-Coordinated Radicals $\mathbf{1}^\bullet$ and $\mathbf{2}^\bullet$ (Oxy Terminus). Both metastable $[\mathbf{1}^\bullet + X]^+$ ions (X = Li or Na) eliminate a $[C,H_3,O]^\bullet$ radical (*m*/*z* 37 or 53, respectively, in insets of Figure 3); the lithiated complex also undergoes $[C,H,O]^\bullet$ loss (*m*/*z* 39). Such products necessitate breakup of the C−C bond in $[\mathbf{1}^\bullet + X]^+$. A plausible pathway involves radical-induced cleavage of this bond to generate the metal ion-bound dimer $^\bullet CH_2OH\cdots X^+\cdots O{=}CH_2$ (**1a**/**1b** in Scheme 2) followed by either direct expulsion of $^\bullet CH_2OH$ or (with Li^+ only) interligand $H^\bullet$ transfer to yield $CH_3OH\cdots X^+\cdots O{=}CH^\bullet$ (**1a′**) and subsequent $OCH^\bullet$ cleavage. This chemistry is similar to that observed for metastable ethylene glycol radical ion, which has been shown to dissociate via the proton-bound complexes $^\bullet CH_2OH\cdots H^+\cdots O{=}CH_2$ and $CH_3OH\cdots H^+\cdots O{=}CH^\bullet$ to $CH_3OH_2^+ + OCH^\bullet$.[34] It is noteworthy that metastable decomposition generates CH_3O-

(34) Ruttink, P. J. A.; Burgers, P. C.; Fell, L. M.; Terlouw, J. K. *J. Phys. Chem. A* **1998**, *102*, 2676−2680.

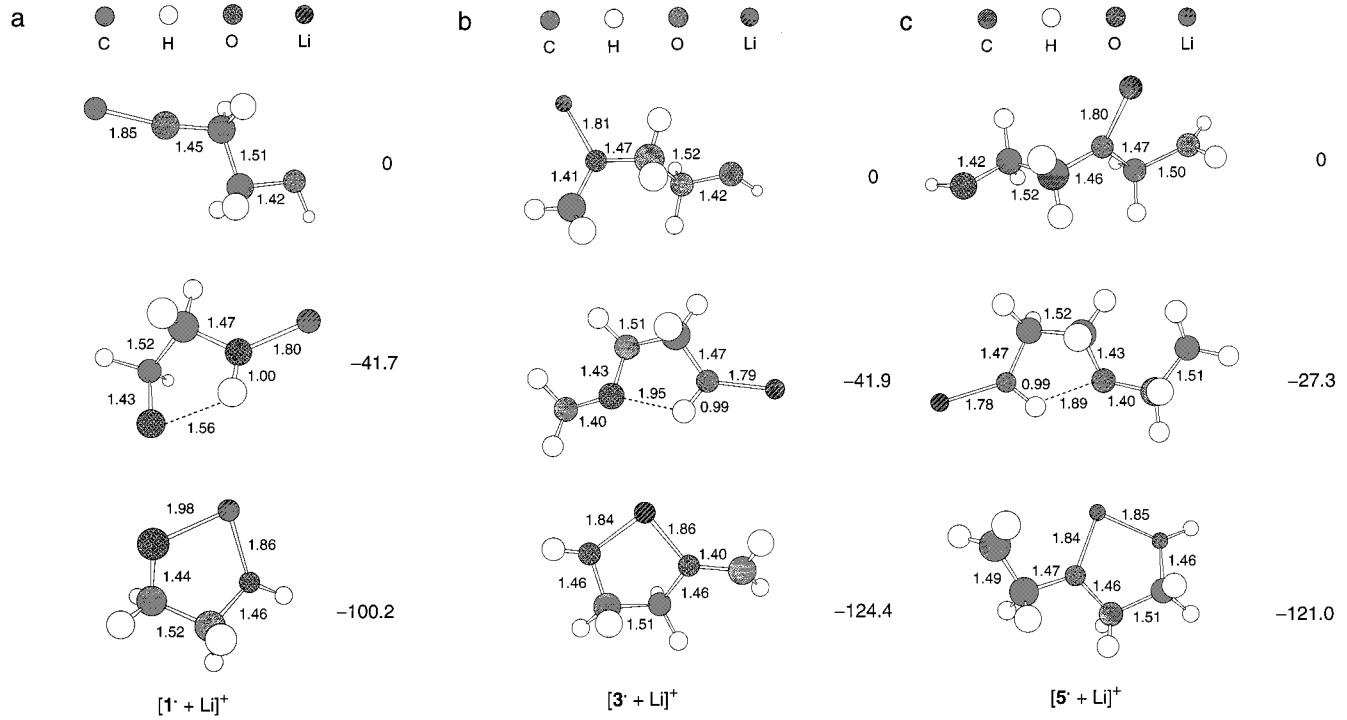

Figure 2. Optimized geometries and relative energies of mono- and bidentate isomers of $[R^\bullet + Li]^+$ ($R^\bullet$ = **1**•, **3**•, **5**•). The bond lengths between heavy atoms are given in Å and the relative energies between isomers are given next to the structures in kJ mol^{-1}; the quoted values include zero-point vibrational corrections. (a) Isomers of lithiated **1**•; (b) isomers of lithiated **2**•; (c) isomers of lithiated **5**•. Top row: Li^+ attachment to ether oxygen or to O•. Middle row: Li^+ attachment to alcohol oxygen. Bottom row: Li^+ attachment to both O sites.

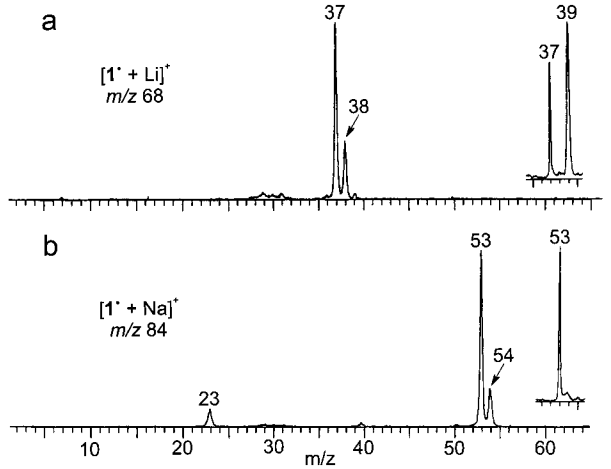

Figure 3. CAD (MS^2) spectra of $[\mathbf{1}^\bullet + X]^+$: (a) X = Li (*m*/*z* 68) and (b) X = Na (*m*/*z* 84). The insets show the corresponding MI spectra. All MI peaks have Gaussian shape and their widths yield $T_{0.5}$ values of 0.1 (*m*/*z* 37), 30 (*m*/*z* 39), and ≤0.1 meV (*m*/*z* 53).

Scheme 2

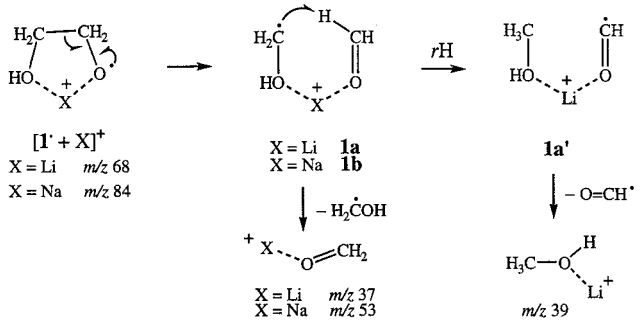

(H)X^+ if X = H and $^+XO{=}CH_2$ if X = Na, and both these fragments if X = Li. In all cases, the products $CH_3O(H)X^+ + OCH^\bullet$ are thermodynamically more stable than $^\bullet CH_2OH + {}^+XO{=}CH_2$.[35−39] The differences originate from substantially different barriers for the formation of $^\bullet CH_2OH\cdots X^+\cdots O{=}CH_2$ and $CH_3OH\cdots X^+\cdots OCH^\bullet$. Ion $HOCH_2CH_2OH^{+\bullet}$ contains an elongated C−C bond (∼2 Å), collapsing to more stable $^\bullet CH_2OH\cdots H^+\cdots O{=}CH_2$.[34] Further isomerization to $CH_3OH\cdots H^+\cdots OCH^\bullet$ proceeds at energies that permit only the formation of $CH_3OH_2^+ + OCH^\bullet$;[34] hence, only this reaction takes place at threshold. On the other hand, the isomerizations $[\mathbf{1}^\bullet + X]^+ \rightarrow$ **1a**/**1b** cleave relatively strong bonds (see C−C bond length in Figure 2), which requires appreciable activation energies (vide infra), thereby making the higher energy dissociation channel ($^+XO{=}CH_2$ formation) accessible to metastable $[\mathbf{1}^\bullet + X]^+$.

Whereas both X^+-bound dimers lose the $O{=}CH_2$ ligand, only the Li^+-containing ion undergoes $OCH^\bullet$ cleavage. This difference is attributed to the higher metal ion−ligand binding energy in **1a** vis à vis **1b**; this increases the lifetime of the former complex, enabling it to attain the geometry needed for interligand H• transfer to the isomeric complex **1a**′, so that $OCH^\bullet$ loss can take place (Scheme 2). If $[\mathbf{1}^\bullet + Li]^+$ is collisionally activated, the internal energy of **1a** is raised, which should

(35) Based on the known heats of formation (kJ mol^{-1}) of $CH_3OH_2^+$ [567],[36] $CH_3O(H)Li^+$ [321],[36,37] $CH_3O(H)Na^+$ [301],[36,38] $OCH^\bullet$ [45],[36] $^\bullet CH_2OH$ [−26],[36] $^+HO{=}CH_2$ [703],[36] $^+LiO{=}CH_2$ [426],[36,39] and $^+NaO{=}CH_2$ [398],[36,38] the products $CH_3O(H)X^+ + OCH^\bullet$ lie lower in energy than the products $^\bullet CH_2OH + {}^+XO{=}CH_2$ by 65, 34, and 26 kJ mol^{-1} for X = H, Li, and Na, respectively.

(36) (a) Linstrom, P. J.; Mallard, W. G., Eds. *NIST Chemistry WebBook*; NIST Standard Reference Database No. 69; National Institute of Standards and Technology: Gaithersburg, MD, November 1998 (http://webbook.nist.gov). (b) Lias, S. G.; Bartmess, J. E.; Liebman, J. F.; Holmes, J. L.; Levin, R. D.; Mallard, W. G. *J. Phys. Chem. Ref. Data* **1988**, *17*, Suppl. No. 1.

(37) Rodgers, M. T.; Armentrout, P. B. *J. Phys. Chem. A.* **1997**, *101*, 2614−2625.

(38) Hoyau, S.; Norman, K.; McMahon, T. B.; Ohanessian, G. *J. Am. Chem. Soc.* **1999**, *121*, 8864−8875.

(39) Wu, J.; Polce, M. J.; Wesdemiotis, C. Unpublished results.

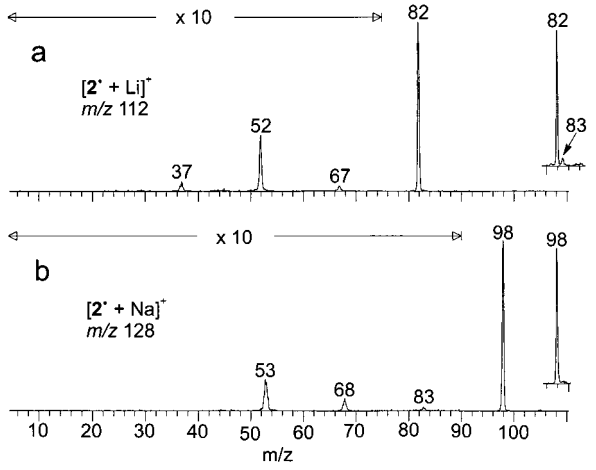

Figure 4. CAD (MS^2) spectra of $[\mathbf{2}^{\bullet} + X]^+$: (a) X = Li (*m*/*z* 112) and (b) X = Na (*m*/*z* 128). The insets show the corresponding MI spectra. All MI peaks have Gaussian shape and their widths yield $T_{0.5}$ values of 4 (*m*/*z* 82), 22 (*m*/*z* 83), and 6 meV (*m*/*z* 98).

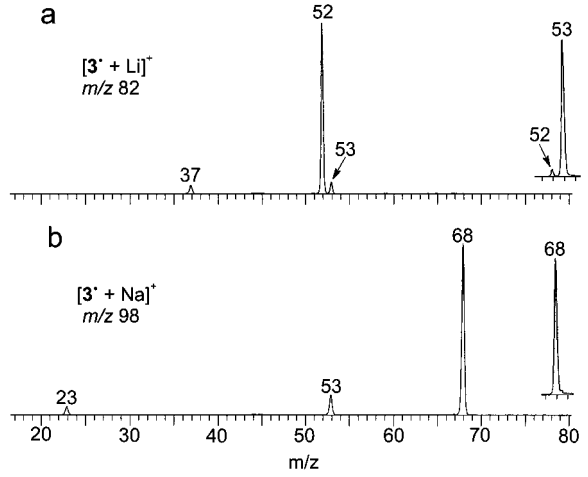

Figure 5. CAD (MS^2) spectra of $[\mathbf{3}^{\bullet} + X]^+$: (a) X = Li (*m*/*z* 82) and (b) X = Na (*m*/*z* 98). The insets show the corresponding MI spectra. All MI peaks have Gaussian shape and their widths yield $T_{0.5}$ values of 8 (*m*/*z* 52), 12 (*m*/*z* 53), and 8 meV (*m*/*z* 68).

Scheme 3

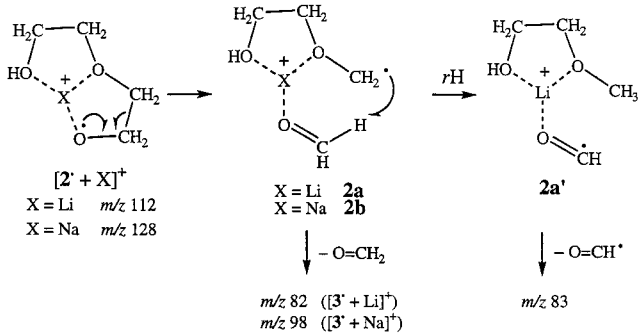

Scheme 4

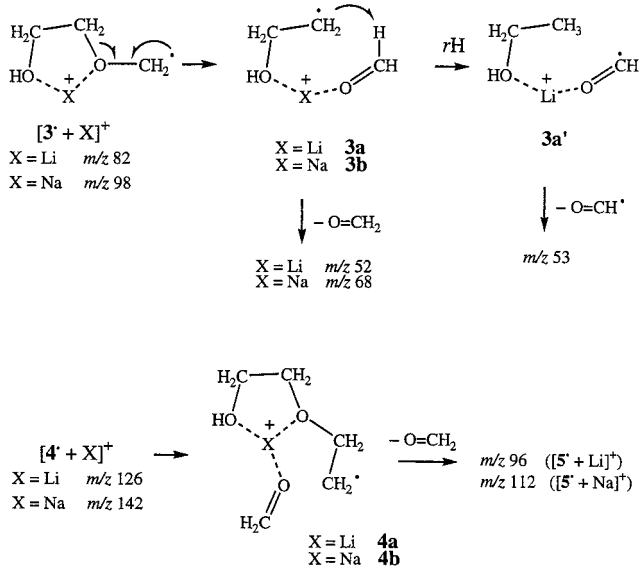

decrease its lifetime[23,24,31] and, thus, the extent of OCH• loss; indeed, this reaction almost disappears in the CAD spectrum (Figure 3a).

In contrast to the MI spectra of $[\mathbf{1}^{\bullet} + X]^+$, the corresponding CAD spectra (Figure 3) show very similar fragmentation patterns, displaying two significant fragment ions from the losses of $HOCH_2^{\bullet}$ (*m*/*z* 37/53 for Li/Na) and $O{=}CH_2$ (*m*/*z* 38/54). Such products can arise by direct cleavages from $[\mathbf{1}^{\bullet} + X]^+$, most likely via the metal ion-bound dimer $^{\bullet}CH_2OH\cdots X^+\cdots O{=}CH_2$ (**1a**/**b**) and subsequent release of either ligand. The lower relative intensities of $^{\bullet}CH_2O(H)X^+$ (*m*/*z* 38/54) vs $^+XO{=}CH_2$ (*m*/*z* 37/53) point out that the hitherto unknown Li^+ and Na^+ affinities of the hydroxymethyl radical are lower than those of formaldehyde which are 145[39] and 96 kJ mol^{-1},[38] respectively.

The analogous, heavier radical cations $[\mathbf{2}^{\bullet} + X]^+$ dissociate in the metastable time window by elimination of formaldehyde; additionally, $[\mathbf{2}^{\bullet} + Li]^+$ loses OCH• (Figure 4, insets). As with the smaller analogues, this behavior can be accounted for by radical site reactions commencing with scission of $O{=}CH_2$ to generate the X^+-bound dimers **2a** or **2b** (Scheme 3). Again, only the lithiated dimer undergoes consecutive interligand H• rearrangement to the isomeric complex **2a′**, from which OCH• can be lost, and this reaction is suppressed during CAD due to an unfavorable entropy.

Collisionally activated $[\mathbf{2}^{\bullet} + X]^+$ show completely parallel characteristics, dissociating extensively by loss of $O{=}CH_2$ to form the smaller metalated radicals $[\mathbf{3}^{\bullet} + X]^+$ (*m*/*z* 82 for Li and 98 for Na). Consecutive $O{=}CH_2$ loss from these major fragments leads to *m*/*z* 52 and 68, respectively (see next section for the chemistry of $[\mathbf{3}^{\bullet} + X]^+$). Other minor CAD products include $^+XO{=}CH_2$ at *m*/*z* 37/53 and the loss of $[C_2,H_5,O]^{\bullet}$ at *m*/*z* 67/83.

Metal Ion-Coordinated Radicals 3• and 4• (Methyl Terminus). Metastable $[\mathbf{3}^{\bullet} + Li]^+$ undergoes two spontaneous decompositions (Figure 5a, inset), involving the losses of formaldehyde (minor channel, *m*/*z* 52) and formyl radical (major channel, *m*/*z* 53). The reaction sequence shown in Scheme 4 (top) resembles that proposed for $[\mathbf{1}^{\bullet} + X]^+$ and $[\mathbf{2}^{\bullet} + X]^+$, starting with a radical-induced cleavage of $O{=}CH_2$ from the polyglycol residue to create the Li^+-bound complex of $^{\bullet}CH_2$-CH_2OH and $O{=}CH_2$ (**3a**); in the second step, the radical site in **3a** abstracts an H• atom from $O{=}CH_2$ to yield complex **3a′**, in which $CH_3CH_2O(H)Li^+$ interacts with the OCH• radical. Subsequent elimination of $O{=}CH_2$ from **3a** or OCH• from **3a′** leads to the observed products (Scheme 4).

The reactivity of metastable $[\mathbf{4}^{\bullet} + Li]^+$ reverses (Figure 6a, inset), with the $O{=}CH_2$ loss (*m*/*z* 96) becoming the principal fragmentation channel. Dissociation through an ion−molecule complex analogous to **3a** can explain this cleavage. In this complex (ion **4a** in Scheme 4), the newly formed $O{=}CH_2$ ligand interacts with a Li^+ ion carrying two instead of one ligand,

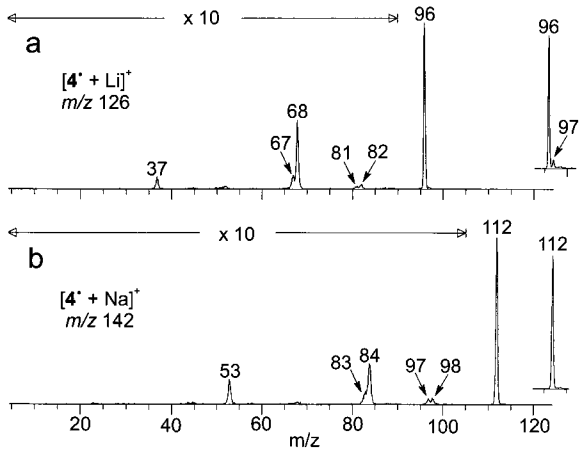

Figure 6. CAD (MS^2) spectra of $[\mathbf{4}^\bullet + X]^+$: (a) X = Li (*m*/*z* 126) and (b) X = Na (*m*/*z* 142). The insets show the corresponding MI spectra. The MI peaks have Gaussian shape and their widths yield $T_{0.5}$ values of 8 (*m*/*z* 96) and 14 meV (*m*/*z* 112); *m*/*z* 97 is not well resolved from *m*/*z* 96 to measure a reliable peak width.

which decreases the electrostatic attraction of O═CH_2 by the metal ion, thereby promoting bond cleavage to *m*/*z* 96 and reducing the extent of H$^\bullet$ rearrangement to *m*/*z* 97. Note that **4a** (from $[\mathbf{4}^\bullet + Li]^+$) and **2a** (from $[\mathbf{2}^\bullet + Li]^+$), which carry similarly coordinated Li^+ ions (tridentate), lose O═CH_2 and OCH$^\bullet$ in a comparable abundance ratio (cf. insets of Figures 4a and 6a).

The only spontaneous reaction of the sodiated radicals $[\mathbf{3}^\bullet + Na]^+$ and $[\mathbf{4}^\bullet + Na]^+$ is loss of O═CH_2 (insets of Figures 5b and 6b). These features agree well with dissociation through the Na^+-bound complexes **3b** and **4b** (Scheme 4) that arise by radical site-initiated cleavage of O═CH_2 in $[\mathbf{3}^\bullet + Na]^+$ and $[\mathbf{4}^\bullet + Na]^+$, respectively. The absence of OCH$^\bullet$ elimination from the sodiated radicals should be due to the weaker binding energy of O═CH_2 to Na^+ within **3b** and **4b**, vis à vis its binding energy to Li^+ within **3a** and **4a**. As indicated above, this reduces the lifetime of **3b**/**4b** (vs **3a**/**4a**), hindering the occurrence of slow rearrangements in them.

For a better understanding of the trends observed in the MI spectra of $[\mathbf{3}^\bullet + X]^+$ and the other radical cations discussed so far, ab initio MO calculations were performed on the parts of the potential energy surfaces of $[\mathbf{3}^\bullet + X]^+$ that are traversed during O═CH_2 loss according to Scheme 4 (top); the results are depicted in Figures 7 and 8. The isomerizations $[\mathbf{3}^\bullet + X]^+ \rightarrow$ **3a**/**b** are found to be exothermic. The higher stabilities of **3a**/**b** vs $[\mathbf{3}^\bullet + X]^+$ are ascribed to a more optimal metal ion coordination by $^\bullet CH_2CH_2OH$ and O═CH_2 than by **3**$^\bullet$ due to a better alignment of the dipole moments of the separate ligands. The activation energy for $[\mathbf{3}^\bullet + X]^+ \rightarrow$ **3a** or **3b** is independent of the metal ion (90 vs 91 kJ mol^{-1} for the two complexes), consistent with no charge involvement in the radical-induced C−O bond cleavages leading to **3a**/**b**. In contrast, the energy needed for elimination of O═CH_2 from **3a**/**b** does depend on X^+ and is significantly smaller for the sodiated than the lithiated complex (89 vs 127 kJ mol^{-1}, respectively). A consequence of these features is that the radical-induced rearrangements $[\mathbf{3}^\bullet + X]^+ \rightarrow$ **3a**/**b** produce **3a** below but **3b** above the dissociation threshold to $^\bullet CH_2CH_2O(H)X^+ +$ O═CH_2 (Figures 7 and 8). Under these circumstances, the sodiated dimer **3b** should decompose immediately and lacks the lifetime needed for further rearrangement to **3b**′ (i.e. $CH_3CH_2OH\cdots Na^+\cdots OCH^\bullet$) for OCH$^\bullet$ loss. Indeed, this reaction is not observed from $[\mathbf{3}^\bullet + Na]^+$ or all other sodiated precursor ions encountered so far. On the other hand, the lithiated dimer **3a** emerging from $[\mathbf{3}^\bullet + Li]^+$ must

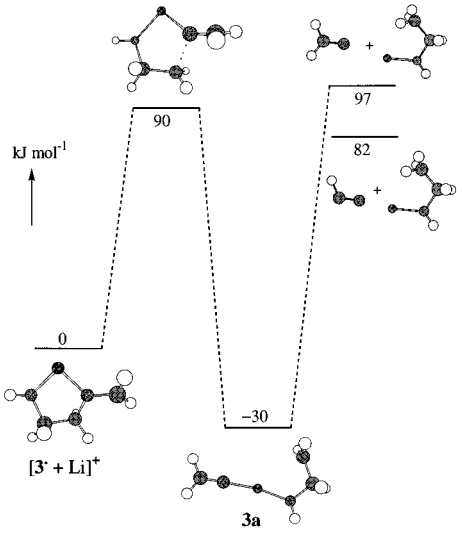

Figure 7. Potential energy diagram for the elimination of O═CH_2 from $[\mathbf{3}^\bullet + Li]^+$ according to Scheme 4. Energy levels are given relative to that of the precursor ion and include zero-point vibrational corrections.

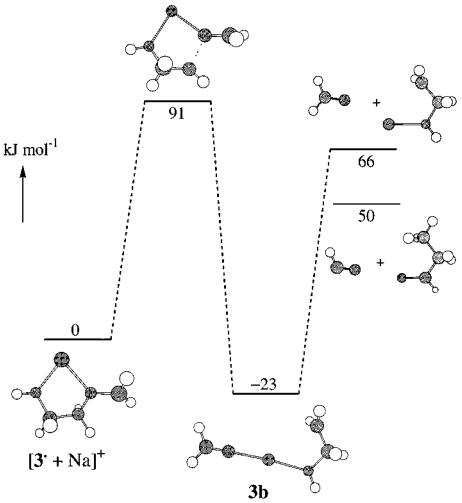

Figure 8. Potential energy diagram for the elimination of O═CH_2 from $[\mathbf{3}^\bullet + Na]^+$ according to Scheme 4. Energy levels are given relative to that of the precursor ion and include zero-point vibrational corrections.

surmount a further barrier for O═CH_2 loss and, hence, should be capable of surviving long enough for the occurrence of the competitive OCH$^\bullet$ elimination.

Due to computational limitations, we were unable to locate the transition state of the interligand H$^\bullet$ transfer **3a** → **3a**′ (Scheme 4). This reaction produces more stable products than the OCH_2 cleavage (Figure 7);[40] since OCH$^\bullet$ loss from $[\mathbf{3}^\bullet + Li]^+$ dominates at threshold, the transition state for **3a** → **3a**′ should lie below 97 kJ mol^{-1}, which is the energy of the rate-determining transition state of the competitive O═CH_2 loss (Figure 7). Overall, the calculations confirm that the extent of OCH$^\bullet$ elimination is mainly determined by the binding energy of O═CH_2 within the X^+-bound dimers of type **a** or **b**. A reduced binding energy and, hence, discrimination against OCH$^\bullet$ loss results by switching the metal ion from Li^+ to Na^+,[37,38] or by increasing the degree of coordination at the Li^+ ion,[28b,41] as observed for $[\mathbf{4}^\bullet + Li]^+$ vs $[\mathbf{3}^\bullet + Li]^+$ as well as $[\mathbf{2}^\bullet + Li]^+$ vs

(40) Transformation of $^\bullet CH_2CH_2O(H)X^+ +$ O═CH_2 to $CH_3CH_2O(H)$-$X^+ +$ OCH$^\bullet$ is exothermic, because it replaces a relatively weak OCH−H bond with a stronger H−CH_2 bond in β-position to a positive charge.[36]

(41) Rodgers, M. T.; Armentrout, P. B. *J. Phys. Chem. A* **1997**, *101*, 1238−1249.

$[\mathbf{1}^{\bullet} + Li]^+$. The calculations also corroborate that the precursor ions produced upon FAB are the cyclic species $[\mathbf{3}^{\bullet} + X]^+$, not the X^+-bound complexes **3a**/**3b**; in the latter case, metastable **3b** would eliminate $OCH^{\bullet}$, which does not take place (no detectable *m*/*z* 69 in the inset of Figure 5b).

Collisional activation of $[\mathbf{3}^{\bullet} + Li]^+$ and $[\mathbf{3}^{\bullet} + Na]^+$ induces very similar unimolecular reactions (Figure 5), the common major decomposition being cleavage of $O{=}CH_2$ to yield the smaller distonic ion $^{\bullet}CH_2CH_2O(H)X^+$ (*m*/*z* 52 with Li^+ and 68 with Na^+). These fragments most likely emerge through the Li^+-bound complexes **3a** and **3b** (Scheme 4), respectively, a proposition supported by the appreciable yield in the CAD spectra of the competitive channel $^{\bullet}CH_2CH_2OH + {}^+XO{=}CH_2$ (*m*/*z* 37 with Li^+ and 53 with Na^+). The only significant difference between lithiated and sodiated $\mathbf{3}^{\bullet}$ is the elimination of $OCH^{\bullet}$ from the former (*m*/*z* 53), which was the principal decomposition of metastable $[\mathbf{3}^{\bullet} + Li]^+$ (vide supra). Note that the yield of $OCH^{\bullet}$ loss decreases markedly from MI to CAD conditions, as also observed for the other lithiated precursors. This decrease attests once more that interligand $H^{\bullet}$ rearrangement (**3a** → **3a′**) is a slow, entropy-constrained process, proceeding efficiently only at threshold energies.

The CAD spectra of the homologous radicals $[\mathbf{4}^{\bullet} + Li]^+$ and $[\mathbf{4}^{\bullet} + Na]^+$ show equivalent fragmentations with strikingly similar relative abundances (Figure 6). The dominant unimolecular reaction is again cleavage of $O{=}CH_2$ which produces the distonic ion $[\mathbf{5}^{\bullet} + X]^+$ (cf. Scheme 4, bottom). Sequential decomposition of the major $[\mathbf{5}^{\bullet} + X]^+$ fragment (see following section for its chemistry) contributes *m*/*z* 81/97, 68/84 ($[\mathbf{1}^{\bullet} + X]^+$), 67/83, and 37/53 ($^+XOCH_2$); the appreciable $^+XOCH_2$ ions can also be formed directly from $[\mathbf{4}^{\bullet} + X]^+$ (via **4a**/**b**) as well as by consecutive cleavage of $HOCH_2^{\bullet}$ from the sizable *m*/*z* 68 and 84 ions, respectively (cf. Figure 3). Finally, the minor CAD products at *m*/*z* 82/98 ($[\mathbf{3}^{\bullet} + X]^+$; X = Li/Na) can be explained by homolysis of the β-bond in respect to the radical site (Scheme 1); their low yield points out that β-bond scission requires a considerably higher critical energy than the favored α-bond cleavages to *m*/*z* 96/112.

The unimolecular chemistry of the charged oxy and methyl radicals discussed so far ($\mathbf{1}^{\bullet}$/$\mathbf{2}^{\bullet}$ and $\mathbf{3}^{\bullet}$/$\mathbf{4}^{\bullet}$, respectively) is dominated by simple cleavages near the radical site to release $O{=}CH_2$ which temporarily stays attached to the metal ion. The emerging metal ion-bound dimer between $O{=}CH_2$ and the remainder of $R^{\bullet}$ undergoes $O{=}CH_2$ expulsion (main channel for heavier analogues $[\mathbf{2}^{\bullet}/\mathbf{4}^{\bullet} + X]^+$) as well as other competitive and consecutive fragmentations whose nature and extent depend on the metal ion and the precursor ion internal energy.

Metal Ion-Coordinated Radicals $\mathbf{5}^{\bullet}$ and $\mathbf{6}^{\bullet}$ (Ethyl Terminus). In this group of $[R^{\bullet} + X]^+$ (Scheme 1), the radical sites are more flexible in approaching other H atoms, which brings upon substantial changes in the ensuing reactivity of these complexes. In the metastable time window (Figure 9, insets), both $[\mathbf{5}^{\bullet} + X]^+$ ions lose $^{\bullet}CH_3$ (*m*/*z* 81/97 for Li/Na) and $^{\bullet}C_2H_5$ (*m*/*z* 67/83);[42] the lithiated ion shows an additional, minor channel, involving the loss of C_2H_4. Upon CAD, $[\mathbf{5}^{\bullet} + X]^+$ still form sizable fragment ions by the loss of methyl and ethyl radicals (Figure 9). Other notable fragments appear at *m*/*z* 68/84 (C_2H_4 loss, basepeaks) and 37/53 ($^+XO{=}CH_2$). The elimination of C_2H_4 corresponds to a direct cleavage of the ethylene side chain, producing the smaller distonic ions $[\mathbf{1}^{\bullet} + X]^+$ (Scheme 5). Consecutive $HOCH_2^{\bullet}$ loss from the latter can yield *m*/*z* 37/53; this proposition is supported by the CAD spectra of authentic $[\mathbf{1}^{\bullet} + X]^+$, which are dominated by *m*/*z* 37/53 (Figure 3).

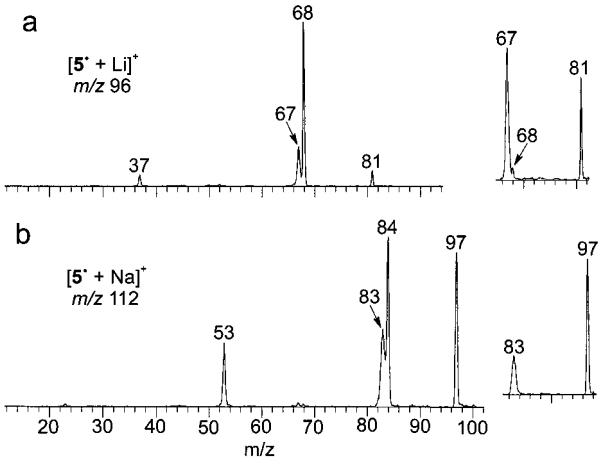

Figure 9. CAD (MS^2) spectra of $[\mathbf{5}^{\bullet} + X]^+$: (a) X = Li (*m*/*z* 96) and (b) X = Na (*m*/*z* 112). The insets show the corresponding MI spectra. The MI peaks have Gaussian shape and their widths yield $T_{0.5}$ values of 70 (*m*/*z* 67), 13 (*m*/*z* 81), 110 (*m*/*z* 83), and 31 meV (*m*/*z* 97).[42]

Scheme 5

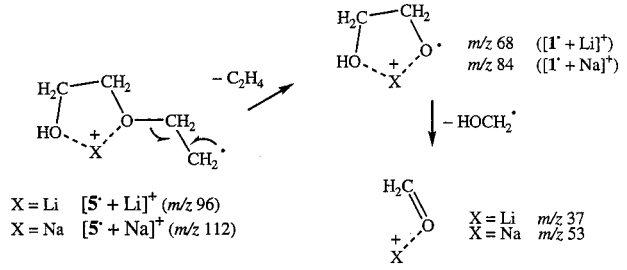

Scheme 6

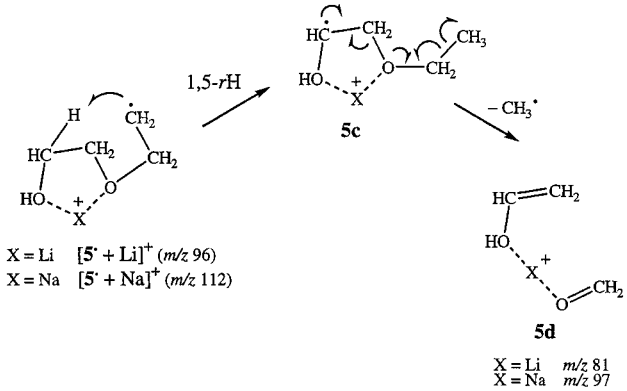

Since the $[\mathbf{5}^{\bullet} + X]^+$ ions do not bear a methyl or ethyl group, the major eliminations of $^{\bullet}CH_3$ and $^{\bullet}C_2H_5$ require prior $H^{\bullet}$ rearrangement. Radicals generally favor 1,4- and 1,5-$H^{\bullet}$ migrations which proceed through five- and six-membered-ring transition states, respectively;[44] such processes are feasible with the polyglycol frame of $\mathbf{5}^{\bullet}$, as illustrated in Schemes 6 and 7. The new radical emerging from 1,5-$H^{\bullet}$ transfer (**5c** in Scheme 6) can initiate a series of simple bond cleavages that ultimately

(42) The much larger kinetic energy release for $^{\bullet}C_2H_5$ loss compared to $^{\bullet}CH_3$ loss (see legend of Figure 9) could be due to the cleavage of an O−C bond during the former vs a C−C bond during the latter process. O−C (or O−H) bond cleavages, followed by elimination of an alkyl radical (or $H^{\bullet}$), are known to have large reverse barriers, resulting in large $T_{0.5}$ values.[43]

(43) (a) Burgers, P. C.; McGibbon, G. A.; Terlouw, J. K. *Eur. Mass Spectrom.* **1995**, *1*, 261−268. (b) Bouma, W. J.; Burgers, P. C.; Holmes, J. L.; Radom, L. *J. Am. Chem. Soc.* **1986**, *108*, 1767−1770.

(44) Wentrup, C. *Reactive Intermediates: The Neutral Reactive Intermediates in Organic Chemistry*; Wiley-Interscience: New York, 1984; pp 23−127.

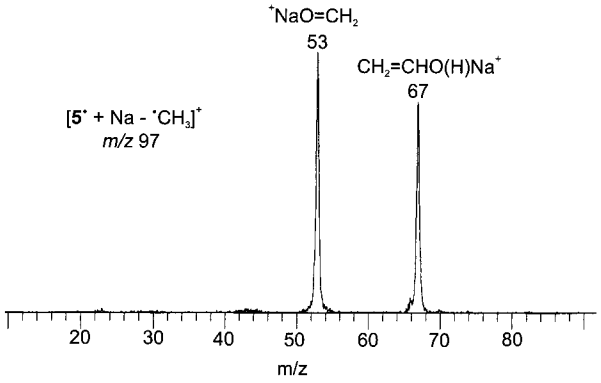

Figure 10. CAD (MS^3) spectrum of [**5**$^\bullet$ + Na − $^\bullet$CH$_3$]$^+$ (*m*/*z* 97) in Figure 9b. It agrees well with structure **5d** (Scheme 6).

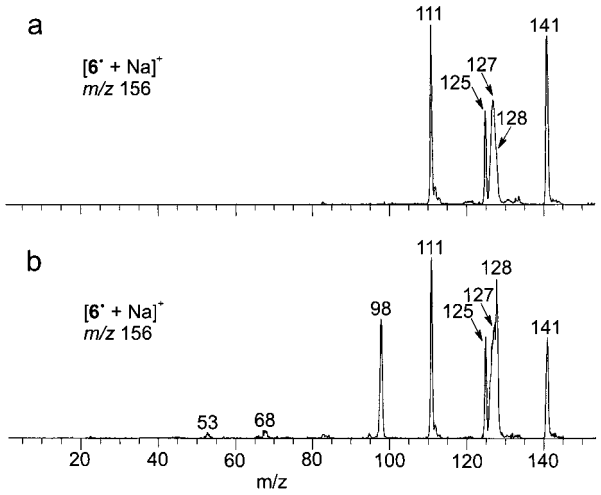

Figure 11. (a) MI and (b) CAD (MS^2) spectra of [**6**$^\bullet$ + Na]$^+$ (*m*/*z* 156). The MI peaks have Gaussian shapes and $T_{0.5}$ values of 11 (*m*/*z* 111), 16 (*m*/*z* 125), ≤220 (*m*/*z* 127), and 66 meV (*m*/*z* 141).[45]

Scheme 7

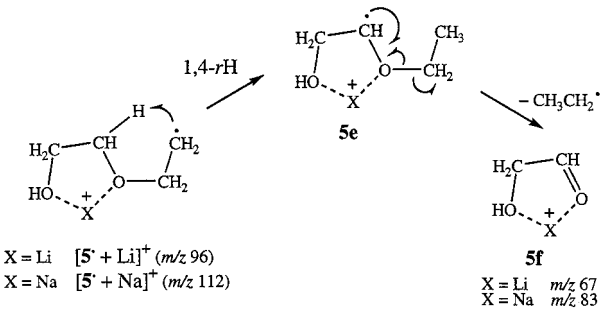

lead to the expulsion of a methyl radical to form the X$^+$-bound complex of CH$_2$═CHOH (vinyl alcohol) and O═CH$_2$ (**5d**). To substantiate this proposal, the MS^3 spectrum of [**5**$^\bullet$ + Na − $^\bullet$CH$_3$]$^+$ was obtained (Figure 10); it basically contains two fragment ions, $^+$NaO═CH$_2$ (*m*/*z* 53) and CH$_2$═CHO(H)Na$^+$ (*m*/*z* 67), in agreement with structure **5d**. The 1,4-H$^\bullet$ rearrangement alternatively moves the radical site to a position that can launch the cleavage of an ethyl radical (Scheme 7). The MS^3 spectrum of the [**5**$^\bullet$ + Na − $^\bullet$C$_2$H$_5$]$^+$ product (not shown) contains fragments at *m*/*z* 23 (100%), 31 (HOCH$_2^+$; 13%), 52 ($^\bullet$CH═ONa$^+$; 23%), and 54 ($^+$Na(H)OCH$_2^\bullet$; 32%), which support the structure **5f** depicted in Scheme 7.

The MI and CAD data of the analogous distonic ions [**6**$^\bullet$ + Li]$^+$ and [**6**$^\bullet$ + Na]$^+$ are qualitatively indistinguishable; only the sodiated radical, which is produced with higher flux and purity, will be presented here. Metastable [**6**$^\bullet$ + Na]$^+$ undergoes

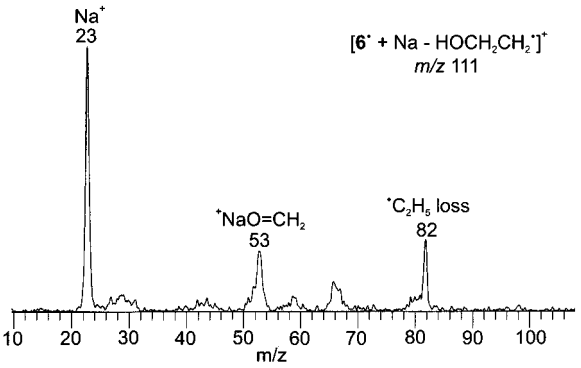

Figure 12. CAD (MS^3) spectrum of [**6**$^\bullet$ + Na − HOCH$_2$CH$_2^\bullet$]$^+$ (*m*/*z* 111) in Figure 11b. It agrees well with structure **6g** (Scheme 9).

Scheme 8

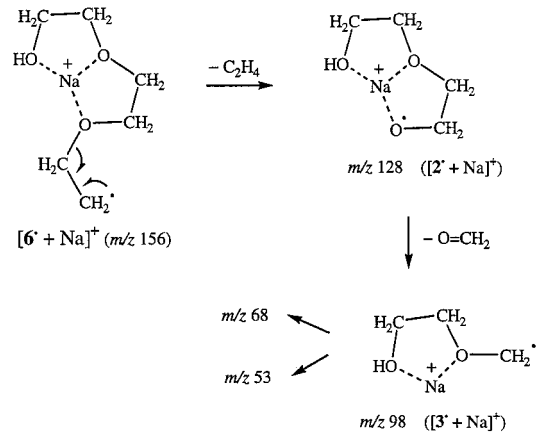

Scheme 9

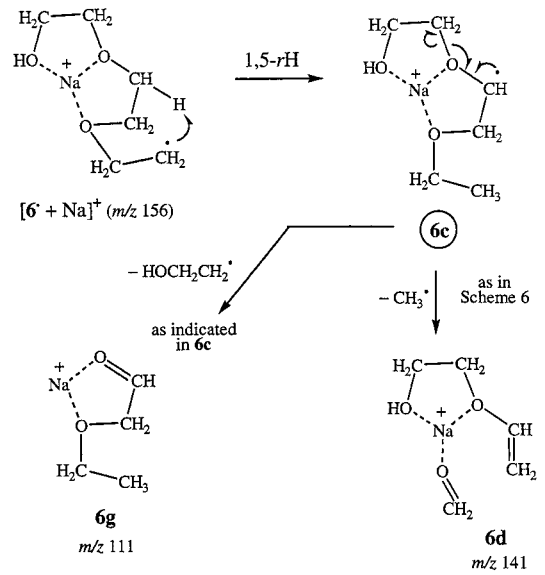

four major competitive dissociations (Figure 11a), leading to the eliminations of $^\bullet$CH$_3$ (*m*/*z* 141), $^\bullet$C$_2$H$_5$ (127), HOCH$_2^\bullet$ (125), and HOCH$_2$CH$_2^\bullet$ (111);[45] an additional, minor channel involves

(45) The losses of $^\bullet$CH$_3$ and (especially) $^\bullet$C$_2$H$_5$ are associated with considerably larger kinetic energy releases than the losses of HOCH$_2^\bullet$ and HOCH$_2$CH$_2^\bullet$ (Figure 11). The $T_{0.5}$ values observed suggest that the reverse barriers of the alkyl eliminations are significant,[42] while those of the hydroxyalkyl eliminations are small or negligible. Compared to $^\bullet$C$_n$H$_{2n+1}$ cleavages, the cleavages of HO(CH$_2$)$_n^\bullet$ remove a potential metal ion binding site, yielding fragments with fewer ligands around the metal ion (cf. Schemes 9 and 10). Such fragments might be sufficiently high in energy that overall reverse barriers become negligible.

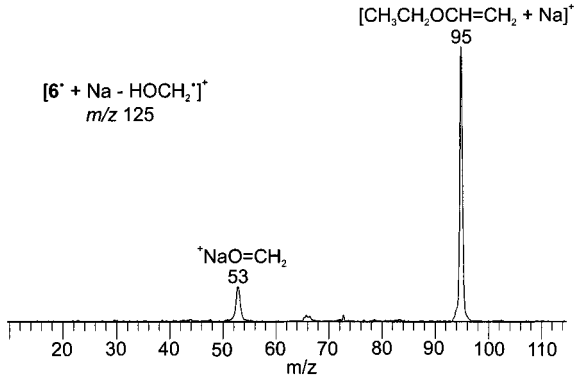

Figure 13. CAD (MS^3) spectrum of $[\mathbf{6}^{\bullet} + Na - HOCH_2^{\bullet}]^+$ (*m*/*z* 125) in Figure 11b. It agrees well with structure **6h** (Scheme 10).

Scheme 10

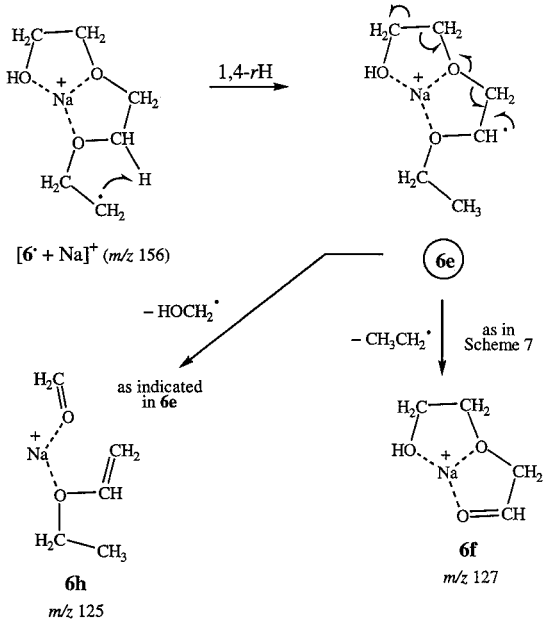

the loss of C_2H_4 (*m*/*z* 128; unresolved from adjacent *m*/*z* 127). The major MI processes continue to proceed abundantly upon CAD (Figure 11b). Collisional activation also enhances substantially the formation of *m*/*z* 128 and 98. The *m*/*z* 128 ion most likely arises by radical-induced cleavage of C_2H_4, which truncates $[\mathbf{6}^{\bullet} + Na]^+$ to the shorter distonic ion $[\mathbf{2}^{\bullet} + Na]^+$ (Scheme 8). Consecutive direct cleavage of $O{=}CH_2$ from $[\mathbf{2}^{\bullet} + Na]^+$ can produce *m*/*z* 98 with the structure $[\mathbf{3}^{\bullet} + Na]^+$; such a sequence is supported by the CAD spectrum of authentic $[\mathbf{2}^{\bullet} + Na]^+$ which is dominated by *m*/*z* 98 (Figure 4b). Similarly, the CAD spectrum of authentic $[\mathbf{3}^{\bullet} + Na]^+$ (Figure 5b) strongly suggests that further decomposition of the *m*/*z* 98 fragment ion is the source of *m*/*z* 68 and (at least partly) of *m*/*z* 53 (Scheme 8).

A 1,5-H$^{\bullet}$ rearrangement in $[\mathbf{6}^{\bullet} + Na]^+$ leads to isomer **6c** (Scheme 9), where the radical can induce the cleavage of either $^{\bullet}CH_3$ (15 u) or $HOCH_2CH_2^{\bullet}$ (45 u) radicals to yield fragment ions **6d** (*m*/*z* 141) and **6g** (*m*/*z* 111), respectively (cf. Figure 11). The MS^3 spectrum of $[\mathbf{6}^{\bullet} + Na - {}^{\bullet}CH_3]^+$ (not shown) is very simple, consisting of peaks at *m*/*z* 53 ($^+NaO{=}CH_2$; 7%) and 111 ($O{=}CH_2$ loss; 100%); these characteristics are in consent with the structure of Na^+-bound dimer **6d**. Similarly, the MS^3 spectrum of $[\mathbf{6}^{\bullet} + Na - HOCH_2CH_2^{\bullet}]^+$ (Figure 12) shows important fragment ions at *m*/*z* 82 ($^{\bullet}C_2H_5$ loss), 53 ($^+NaO{=}CH_2$), and 23 (Na^+), which are in consent with the connectivity **6g**.[46]

A 1,4-H$^{\bullet}$ rearrangement in $[\mathbf{6}^{\bullet} + Na]^+$, on the other hand, creates the isomeric distonic radical cation **6e** (Scheme 10). This can initiate the cleavage of ethyl to produce **6f** (*m*/*z* 127; an analogue of **5f** in Scheme 7). An alternative direct cleavage can progress toward the opposite direction, expelling a hydroxymethyl radical from the other terminus to yield ion **6h** (*m*/*z* 125), the Na^+-bound complex of formaldehyde, and ethyl vinyl ether. Corroborative evidence for this pathway is provided by the MS^3 spectrum of $[\mathbf{6}^{\bullet} + Na - HOCH_2^{\bullet}]^+$ (Figure 13), which is dominated by the sodiated monomers of **6h**, viz. $^+NaO{=}CH_2$ (*m*/*z* 53) and $[CH_3CH_2OCH{=}CH_2 + Na]^+$ (*m*/*z* 95).

Conclusions

Distonic $[R^{\bullet} + X]^+$ ions with sufficient internal energy to decompose undergo typical radical site decompositions, viz. direct cleavages in the α-position to the radical center and 1,4- or 1,5-H$^{\bullet}$ rearrangements. Although these reactions are induced by the unpaired electron, the metal ion is not just a spectator. It rather acts as a mediator, promoting or hindering certain pathways. The metal ion accomplishes these tasks by disabling bond rotations in the R$^{\bullet}$ segment involved in the coordination of the metal ion, so that the radical site cannot abstract nearby H atoms; as a charged particle, the metal ion also makes possible the formation of ion−molecule complexes, in which cleaved molecules with heteroatoms continue to interact with the metal. Interligand H$^{\bullet}$ transfer may take place in the latter complexes, depending on their lifetimes which in turn are influenced by the X^+-ligand binding energies.

Our studies are currently expanded to probe metalated radicals derived from crown ethers (they are more unsaturated as compared to the $[R^{\bullet} + X]^+$ ions discussed here), metal ion-coordinated peptide radicals (of biological interest),[47] and the ion−molecule reactions of $[R^{\bullet} + X]^+$ with double-bond-containing reagents (which confirm the distonic nature of the metalated radicals).[48]

Acknowledgment. We thank Dr. David A. Modarelli for helpful discussions. We are grateful to the National Science Foundation (CHE-9725003) for generous financial support.

JA0020660

(46) The latter MS^3 data also reveal that $[\mathbf{6}^{\bullet} + Na - 45]^+$ (*m*/*z* 111 in Figure 11) is *not* formed in any significant extent by successive losses of $CH_3^{\bullet} + O{=}CH_2$ (i.e. through **6c** and **6d**) or by elimination of $^{\bullet}OCH_2CH_3$ from **6c**; in such a case, $[\mathbf{6}^{\bullet} + Na - 45]^+$ would have had the structure $[HOCH_2CH_2OCH{=}CH_2 + Na]^+$ (i.e. $[\mathbf{6d} - O{=}CH_2]^+$) which is incompatible with the MS^3 spectrum of Figure 12.

(47) Talley, J. M.; Polce, M. J.; Wesdemiotis, C. Proceedings of the 47th ASMS Conference, June 13−17, 1999, Dallas, TX, WOD 11:15.

(48) Talley, J. M.; Polce, M. J.; Wesdemiotis, C. Proceedings of the 48th ASMS Conference, June 11−15, 2000, Long Beach, CA, MOF 11:15.